

LRF-Net: Learning Local Reference Frames for 3D Local Shape Description and Matching

Angfan Zhu, Jiaqi Yang, Chen Zhao, Ke Xian, Zhiguo Cao* and Xin Li

Abstract

The local reference frame (LRF) acts as a critical role in 3D local shape description and matching. However, most of existing LRFs are hand-crafted and suffer from limited repeatability and robustness. This paper presents the first attempt to learn an LRF via a Siamese network that needs weak supervision only. In particular, we argue that each neighboring point in the local surface gives a unique contribution to LRF construction and measure such contributions via learned weights. Extensive analysis and comparative experiments on three public datasets addressing different application scenarios have demonstrated that LRF-Net is more repeatable and robust than several state-of-the-art LRF methods (LRF-Net is only trained on one dataset). In addition, LRF-Net can significantly boost the local shape description and 6-DoF pose estimation performance when matching 3D point clouds.

1 Introduction

The local reference frame (LRF) is a canonical coordinate system established in the 3D local surface, which is a useful geometric cue for 3D point clouds. LRF possesses two intriguing traits. One is that rotation invariance can be achieved via LRF if the local surface is transformed with respect to the LRF [Guo *et al.*, 2013]. The other is that useful geometric information can be mined with LRF [Petrelli and Di Stefano, 2011]. These make LRF popular in many geometric relevant tasks, especially for local shape description and six-degree-of-free (6-DoF) pose estimation.

For local shape description, two corresponding local surfaces can be converted into the same pose and full 3D geometric information can be employed, which is beneficial to improving the performance of local descriptors. Some hand-crafted local shape descriptors, e.g., signature of histograms of orientations (SHOT) [Tombari *et al.*, 2010] and signature of rotational projection statistics (RoPS) [Guo *et al.*, 2013], estimate an LRF from the local surface and then translate local geometric information with respect to the estimated LRF

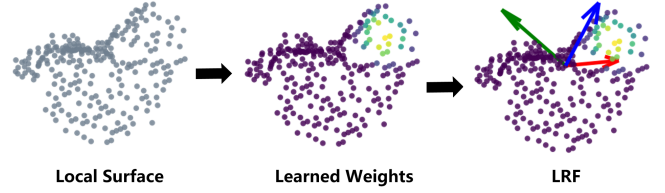


Figure 1: LRF-Net first assigns learned weights to points in a local surface and then using these weights to estimate a repeatable and robust LRF.

into distinctive and rotation-invariant feature representations. Some learned local descriptors, e.g., [Gojcic *et al.*, 2019] and [Spezialetti *et al.*, 2019], leverage LRFs to overcome the limitation of geometric deep learning networks of being sensitive to rotations. Therefore, LRF is critical for both traditional and learned local shape descriptors. For 6-DoF pose estimation, an LRF can significantly improve its efficiency. Traditional 6-DoF pose estimation is usually performed via RANSAC [Derpanis, 2010], which randomly selects inlier correspondences from an initial correspondence pool to for pose prediction. Such random sampling method is neither reliable nor computationally efficient [Deng *et al.*, 2019]. By contrast, we can directly predict an initial pose via two corresponding LRFs, reducing the computational complexity from $O(n^3)$ to $O(n)$.

The desirable properties for LRF are twofold [Tombari *et al.*, 2010]. The first one is the invariance to rigid transformation (e.g., translations and rotations). The second one is the robustness to common disturbances (e.g., noise, clutter, occlusion and varying mesh resolutions). To achieve these goals, many LRF methods have been proposed in the past decade and they can be categorized into two classes [Yang *et al.*, 2018]: covariance analysis (CA) [Mian *et al.*, 2010; Tombari *et al.*, 2010] or point spatial distributions (PSD)-based [Petrelli and Di Stefano, 2011; Petrelli and Di Stefano, 2012; Yang *et al.*, 2017]. CA-based LRFs are based on the computation of eigenvectors of a covariance matrix calculated either for the points or triangles in the local surface. PSD-based LRFs usually calculate estimate axes successively, where the main efforts are put on the determination of the x -axis [Yang *et al.*, 2018]. However, most CA-based LRFs still suffer from sign ambiguity, and PSD-based LRFs

*Contact Author

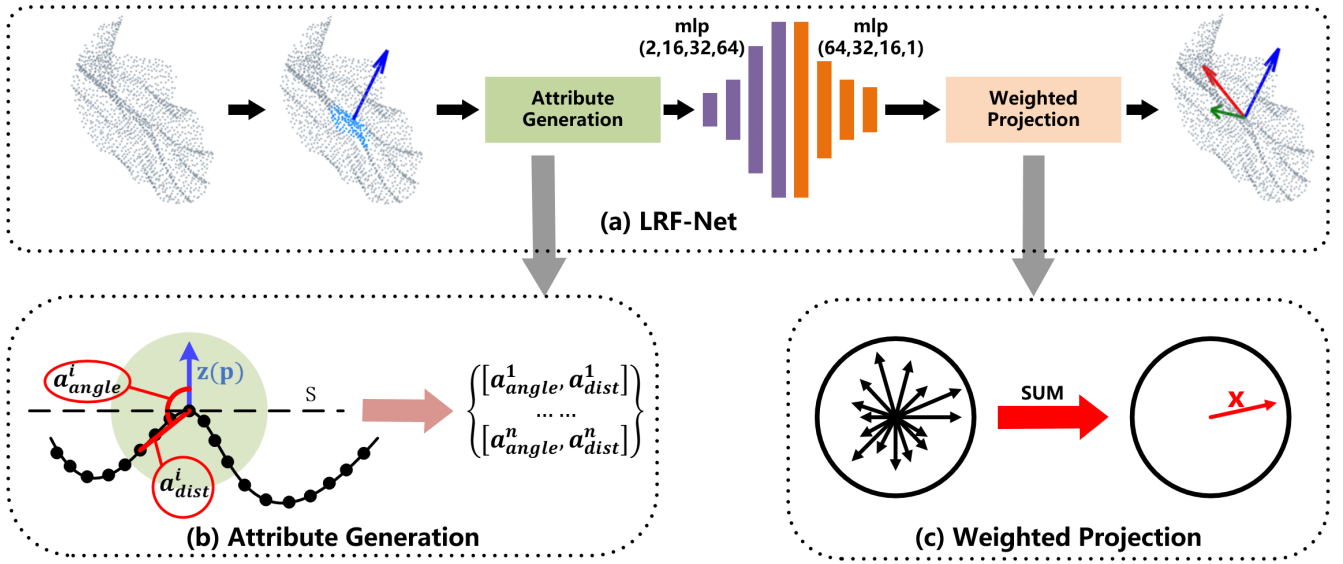


Figure 2: The architecture of LRF-Net. The input to LRF-Net is a local surface and we calculate its normal as the z -axis of the LRF. Then, the local surface is converted to a set of rotation variant attributes. Next, a projection weight for every point is computed with mlp. At last, x -axis is calculated by the weighted vector-sum of all the projection vectors and the y -axis is calculated by the cross product between z -axis and x -axis. The LRF is formed as the combination of x -axis, y -axis and z -axis.

show limited robustness to high levels of noise and variations of mesh resolution [Petrelli and Di Stefano, 2012]. Methods in both classes usually apply a weighted strategy to improve their repeatability performance. However, their weights are determined heuristically, and the repeatability performance in challenging 3D matching cases cannot be guaranteed.

Motivated by existing considerations, we propose a learned approach toward LRF estimation (named LRF-Net), which considers the contribution of all neighboring points (Fig. 1). Our key insight is that each neighboring point in the local surface gives a unique contribution to LRF construction, which can be quantitatively represented by assigning weights to these points. Given a local surface centered at a keypoint, we first resort to the normal of the keypoint computed within a subset of the radius neighbors for the calculation of its z -axis. Its repeatability has been confirmed in [Petrelli and Di Stefano, 2011]. Compared with z -axis, estimating the x -axis is more challenging, due to noise, clutter, and occlusion. By collecting angle and distance attributes within a local neighborhood, we can formulate the estimation of x -axis as a weighted prediction problem with respect to these geometric attributes. Unlike previous CA-based and PSD-based approaches, such learned strategy of determining weights is shown to be invariant to rigid transformation and robust to noise, clutter, occlusion and varying mesh resolutions. Our network can be trained in a weakly supervised manner. Specifically, it needs the corresponding relationships between local patches only, instead of ground-truth LRFs and/or exact pose variation information between patches. We have conducted a set of experiments on three public datasets to comprehensively evaluate the proposed LRF-Net. Extensive analysis and comparative experiments on three public datasets addressing different application scenarios have

demonstrated that LRF-Net is more repeatable and robust than several state-of-the-art LRF methods (LRF-Net is only trained on one dataset). In addition, LRF-Net can significantly boost the local shape description and 6-DoF pose estimation performance when matching 3D point clouds. The major contributions of this paper are summarized as follows:

- LRF-Net, based on a Siamese network that needs weak supervision only, is proposed that achieves the state-of-the-art repeatability performance under the impacts of noise, varying mesh resolutions, clutter and occlusion. To the best of our knowledge, we are the first to concentrate on designing LRF for local surfaces with deep learning.
- LRF-Net can significantly boost the performance of local shape description and 6-DoF pose estimation.

The rest of this paper is organized as follows. Section 2 presents a detailed description of our proposed LRF-Net. Section 3 presents the experimental evaluation of LRF-Net on three public datasets with comparisons with several state-of-the-art methods. Several concluding remarks are drawn in Section 4.

2 Method

This section represents the details of our proposed LRF-Net for 3D local surface. We first introduce the technique approach for calculating the three axes for an LRF and then describes a weakly supervised approach for training LRF-Net.

2.1 A Learned LRF Proposal

The whole architecture of LRF-Net is shown in Fig. 2(a). LRF-Net predicts the direction of three axes successively. For a local surface, we first estimate its z -axis via its normal

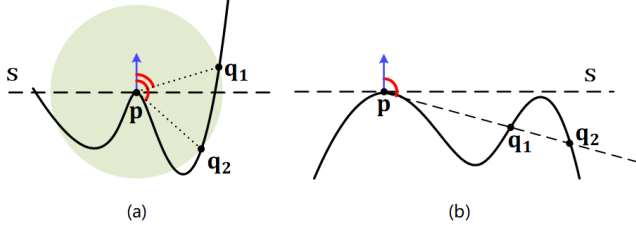


Figure 3: An illustration of information complementary inherent to the two attributes in LRF-Net. The two radius neighbors \mathbf{q}_1 and \mathbf{q}_2 of the keypoint \mathbf{p} in (a) and (b) have different spatial locations. In (a), the two radius neighbors with the same distance value are distinguished by the surface variation angle attribute. In (b), their surface variation angle attribute values are similar, while can be distinguished by the distance attribute.

vector computed over a small subset of the local point set. Then, unique weights are learned for each point in the local surface. The x -axis is calculated by integrating projection vectors with learned weights using a vector-sum operation. At last, the y -axis is calculated by the cross-product operation between z -axis and x -axis.

LRF definition: Given a local surface \mathbf{Q} centered at keypoint \mathbf{p} , the LRF at \mathbf{p} (denoted by $\mathbf{L}_\mathbf{p}$) can be represented as :

$$\mathbf{L}_\mathbf{p} = [\mathbf{x}(\mathbf{p}), \mathbf{z}(\mathbf{p}) \times \mathbf{x}(\mathbf{p}), \mathbf{z}(\mathbf{p})], \quad (1)$$

where $\mathbf{x}(\mathbf{p})$, $\mathbf{y}(\mathbf{p})$, and $\mathbf{z}(\mathbf{p})$ denote the x -axis, y -axis, and z -axis of $\mathbf{L}_\mathbf{p}$, respectively. As three axes are orthogonal, the estimation of LRF therefore contains two parts: estimation of the z -axis and the x -axis.

A naive way to learn an LRF for the local surface is to train a network that directly regresses the axes. The premise is that ground-truth LRFs are labeled for local surfaces. Unfortunately, the network trained in this manner meets two difficulties. The first one is that the definition of ground-truth LRFs for local surfaces remain an open issue in the community [Yang *et al.*, 2018]. The second one, which is more important, is that the orthogonality of three axes cannot be guaranteed. We suggest estimating z -axis and x -axis independently.

z -axis: As for z -axis, we take the normal of the key-point as the z -axis., which has been confirmed [Petrelli and Di Stefano, 2011] to be quite repeatable. To resist the impact fo clutter and occlusion, we collect a small subset of the local surface to calculate the normal. For more details, readers are referred to [Yang *et al.*, 2017].

x -axis: Once the z -axis is determined, the remaining task is to compute the x -axis. Compared with z -axis, x -axis is more challenging due to noise, clutter, and occlusion [Yang *et al.*, 2018]. We argue that each neighboring point in the local surface gives a unique contribution to LRF construction. Hence, we predict a weight for each neighboring point and leverage all neighboring points with learned weights for x -axis prediction. The main steps are as follows. First, to make the estimate LRF invariant to rigid transformation, our

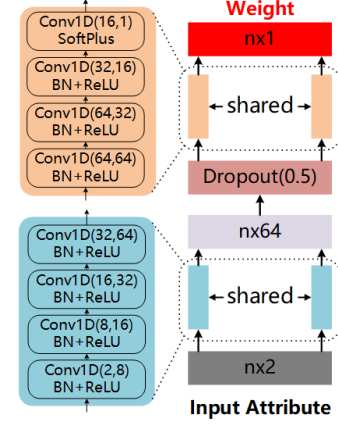


Figure 4: Parameters of our LRF-Net.

network consumes with invariant geometric attributes, rather than point coordinates. In particular, two attributes, i.e., relative distance a_{dist} and surface variation angle a_{angle} are used in LRF-Net as illustrated in Fig. 2(b). For a neighbor \mathbf{q}_i of \mathbf{p} , the two attributes of \mathbf{q}_i are computed as:

$$\begin{cases} a_{dist}^i = \|\mathbf{p}\mathbf{q}_i\| / r \\ a_{angle}^i = \cos(\mathbf{z}(\mathbf{p}), \mathbf{p}\mathbf{q}_i) \end{cases}, \quad (2)$$

where $\|\cdot\|$ is the L_2 norm and r represents the support radius of the local surface. The range of a_{angle} and a_{dist} are $[-1, 1]$ and $[0, 1]$, respectively. Thus, every radius neighboring point represented by two attributes that will be encoded to a weight value via LRF-Net later. The employed two attributes in LRF-Net have two merits at least. First, the unique spatial information of a radius neighboring point in the local surface can be well represented, as shown in Fig. 3. Both attributes are complementary to each other. Second, the two attributes are calculated with respect to the keypoint, which are rotation invariant. It makes the learned weights rotation invariant as well. Second, with geometric attributes being the input, we use a U-Net with multilayer perceptions (MLP) layers only to predict weights for neighboring points. The details of the network are illustrated in Fig. 4. The network is very simple, however, is sufficient to predict stable and informative weights for neighboring points (as will be verified in the experiments).

Third, because x -axis is orthogonal to z -axis, we project each neighbor \mathbf{q}_i on the tangent plane \mathbf{S} of the z -axis and compute a projection vector for \mathbf{q}_i as:

$$\mathbf{v}_i = \mathbf{p}\mathbf{q}_i - (\mathbf{p}\mathbf{q}_i \cdot \mathbf{z}(\mathbf{p})) \cdot \mathbf{z}(\mathbf{p}). \quad (3)$$

We integrate all weighted projection vectors in a weighted vector-sum manner:

$$\mathbf{x}(\mathbf{p}) = \sum_{i=1}^n w_i \mathbf{v}_i / \left\| \sum_{i=1}^n w_i \mathbf{v}_i \right\|, \quad (4)$$

where n denotes the total number of radius neighbors of keypoint \mathbf{p} and w_i is a learned weight by LRF-Net. Another way for determining the x -axis, based on these weights,

is choosing the vector with the maximum weight, as in many PSD-based LRFs [Petrelli and Di Stefano, 2011; Petrelli and Di Stefano, 2012]. However, it fails to leverage all neighboring information and we will show that it is inferior to the vector-sum operation in the experiments.

y-axis: Based on the calculated z -axis and x -axis, the y -axis can be computed by the cross-product between them.

2.2 Weakly Supervised Training Scheme

Our training data are constituted by a series of corresponding local surface patches. The corresponding relationship is obtained based on the ground-truth rigid transformation of two whole point clouds. In particular, LRF-Net needs the corresponding relationships between local surface patches only, rather than ground-truth LRFs and/or exact pose variation information between patches. Therefore, our network can be trained in a weakly supervised manner.

We train our LRF-Net with two streams in a Siamese fashion where each stream independently predicts an LRF for a local surface. Specifically, two streams take the local surfaces of keypoints \mathbf{p}_m and \mathbf{p}_s as inputs, respectively. Here, \mathbf{p}_m and \mathbf{p}_s are two corresponding keypoints sampled from the model and scene point cloud. Both streams share the same architecture and underlying weights. We use the predicted LRFs \mathbf{L}_m and \mathbf{L}_s by two stream to transform the local surfaces \mathbf{Q}_m and \mathbf{Q}_s to the coordinate system of the two LRFs. Then, we calculate the Chamfer Distance [Deng *et al.*, 2018] between two transformed local surfaces as the loss function to train LRF-Net:

$$Loss = d_{cham}(\mathbf{L}_m \cdot \mathbf{Q}_m, \mathbf{L}_s \cdot \mathbf{Q}_s), \quad (5)$$

where

$$d_{cham}(X, \hat{X}) = \min \left\{ \frac{1}{|X|} \sum_{x \in X} \min_{\hat{x} \in \hat{X}} \|x - \hat{x}\|, \frac{1}{|\hat{X}|} \sum_{\hat{x} \in \hat{X}} \min_{x \in X} \|x - \hat{x}\| \right\}. \quad (6)$$

Remarkably, our opinion is that it is difficult to define a “good” LRF for a single local surface. For 3D shape matching, LRFs that can align the poses of two local surface patches are judged as repeatable. This motivates us to consider two local patches simultaneously and employ the Chamfer Distance to train the network.

3 Experiments

In this section, we first evaluate the repeatability performance of our LRF-Net on three standard datasets, including the Bologna retrieval (BR) dataset [Tombari *et al.*, 2013], the UWA 3D modeling (UWA3M) dataset [Mian *et al.*, 2006b], and the UWA object recognition (UWAOR) dataset [Mian *et al.*, 2006a], together with a comparison with other state-of-the-art LRFs. Second, we apply our LRF-Net perform local shape description and 6-DoF pose estimation to verify the practicability of our method. Third, analysis experiments are conducted to improve the explainability of the proposed LRF-Net.

Table 1: Experimental datasets and inherited properties

Dataset	BR	UWA3M	UWAOR
Scenario	Retrieval	Registration	Recognition
Challenge	Gaussian noise	holes, missing region, and self-occlusion	clutter and occlusion
# Models	6	4	5
# Scenes	18	75	50
# Matching Pairs	18	75	188

3.1 Experimental Setup

The details of our experiments including the description of datasets and the illustration for all compared methods are introduced before evaluation. The experiments were conducted on a Windows Server with an Intel Xeon E5-2640 2.39 GHz CPU and 96 GB of RAM. We train our LRF-Net using a batch size of 512 local surface pairs and leverage the ADAM optimizer with an initial learning rate of $1e-4$, which decays 5% every epoch. Each sampled local surface contains 256 points. The max epoch count is set to 20.

Datasets

Our experimental datasets includes three standard datasets with different application scenarios. The variety among these public 3D datasets definitely helps us to evaluate the performance of our method in a comprehensive manner. The main properties of these datasets are summarized in Table 1.

These dataset are also injected with five levels of Gaussian noise (i.e., from 0.1 mr to 0.5 mr Gaussian noise) and four levels of mesh decimation (i.e., $\frac{1}{2}$, $\frac{1}{4}$, $\frac{1}{8}$ and $\frac{1}{16}$ of original mesh resolution). Here, the unit mr denotes mesh resolution. Remarkably, *the noise-free BR dataset is used to train our LRF-Net, the rest noisy data in the BR dataset and data in the UWA3M dataset and the UWAOR dataset are used for testing.*

Compared Methods

We compare our LRF-Net with several existing LRF methods for a through evaluation. Specifically, the compared methods are proposed by Mian *et al.* [Mian *et al.*, 2010], Tombari *et al.* [Tombari *et al.*, 2010], Petrelli *et al.* [Petrelli and Di Stefano, 2012], Guo *et al.* [Guo *et al.*, 2013] and Yang *et al.* [Yang *et al.*, 2017], respectively. We dub them as *Mian*, *Tombari*, *Petrelli*, *Guo*, and *Yang*, respectively. To compare fairly, we keep the support radius of all the LRFs as 15 mr. The properties of these LRFs are shown in Table 2.

To evaluate the local shape description performance of our method, we replace the LRF in four LRF-based descriptors (i.e., snapshots [Malassiotis and Srinivas, 2007], SHOT [Tombari *et al.*, 2010], RoPS [Guo *et al.*, 2013] and TOLDI [Yang *et al.*, 2017]) and assess the performance variations. To measure the 6-DoF pose estimation performance of our method, we adapt LRF-Net to the RANSAC pipeline and compare with the original RANSAC [Fischler and Bolles, 1981].

3.2 Performance Evaluation of LRF-Net

Repeatability Performance

We evaluate the repeatability of all LRFs via the popular *MeanCos* [Tombari *et al.*, 2010] metric, which measures

Table 2: Properties of six LRF methods. H and L respectively represent hand-crafted and learned methods for point weight calculation; P and M respectively denote point cloud and mesh.

Method	<i>Mian</i>	<i>Tombari</i>	<i>Guo</i>	<i>Petrelli</i>	<i>Yang</i>	<i>Ours</i>
Category	CA	CA	CA	PSD	PSD	PSD
Date type	P	P	M	P	P	P
Weight	—	H	H	H	H	L

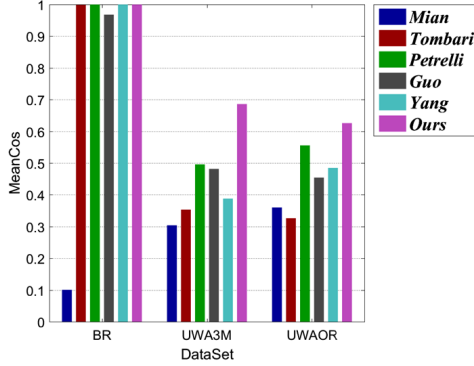


Figure 5: Repeatability performance of six LRF methods on the BR, UWA3M, and UWAOR datasets.

overall angular error between two LRFs. The repeatability results of evaluated LRFs are shown in Fig. 5 and Fig. 6. Several observations can be made from these figures.

First, as witnessed by Fig. 5, our LRF together with *Tombari*, *Petrelli*, and *Yang* achieve decent performance on the BR dataset. On the UWA3M and UWAOR datasets, our LRF-Net achieves the best performance. Second, as shown in Fig. 6(a), LRF-Net and *Tombari* achieve a comparably stable performance on the BR dataset with respect to different levels of Gaussian noise. Fig. 6(b) and Fig. 6(c) indicate that LRF-Net achieves the best performance under all levels of Gaussian noise on the UWA3M and UWAOR datasets, surpassing the others by a very significant gap. Note that UWA3M and UWAOR datasets also include nuisances such as clutter, self-occlusion, and occlusion. Third, results in Fig. 6(d)-(f) suggest that LRF-Net is the best competitor with $\frac{1}{2}$, $\frac{1}{4}$, and $\frac{1}{8}$ mesh decimation on all datasets.

These results clearly demonstrate the strong robustness of our LRF-Net with respect to Gaussian noise, mesh decimation, clutter, and occlusion. The reasons are at least twofold. One is that all points are leveraged to generate the critical x -axis, which guarantees the robustness to Gaussian noise and low level mesh decimation. The other is that a LRF-Net can learn stable and informative weights for neighboring points. It can improve the robustness of LRF-Net to common nuisances.

Local Shape Description Performance

We further evaluate our LRF-Net by replacing the LRFs in four LRF-based descriptors (i.e., snapshots, SHOT, RoPS, and TOLDI) with our LRF-Net. Then we compare their descriptor matching performance measured via recall vs. 1-precision curve (RPC) [Guo *et al.*, 2016; Tombari *et al.*, 2010]. Notably, the original LRF methods employed by snap-

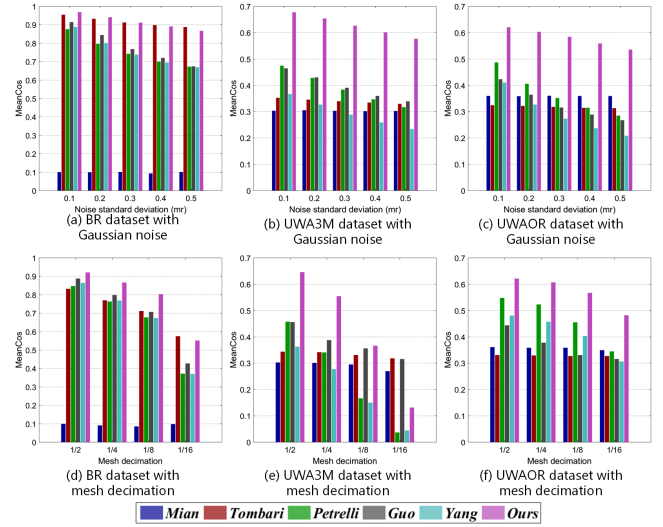


Figure 6: Robustness performance of six LRF methods on the BR, UWA3M, and UWAOR datasets with Gaussian noise and mesh decimation.

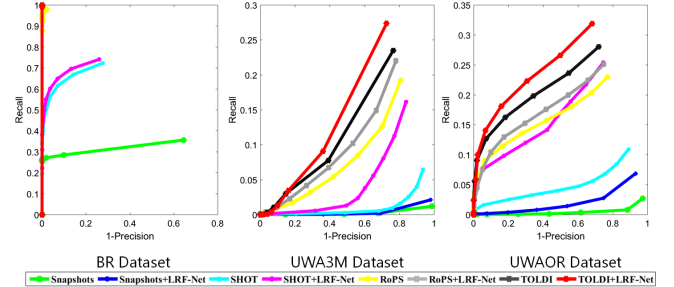


Figure 7: Local shape description performance of LRF-based descriptors with LRF-Net and their original LRFs on the BR, UWA3M, and UWAOR datasets.

shots, SHOT, RoPS, and TOLDI are *Mian*, *Tombari*, *Guo* *Yang*, respectively. We conduct this experiment on the original BR, UWA3M, and UWAOR datasets. Fig. 7 reports the RPC results of the all tested descriptors.

As witnessed by the figure, all LRF-based descriptors equipped with our LRF-Net outperform their original versions. Specifically, snapshots achieve a dramatic performance improvement with our LRF-Net on the BR dataset; the performance of SHOT also climbs significantly on the UWA3M and UWAOR datasets with the help of the proposed LRF-Net. Therefore, we can draw a conclusion that LRF plays an important role in local shape description, where a repeatable LRF can effectively improve the description performance of an LRF-based descriptor without changing its feature representation. It also indicates that the proposed LRF-Net can bring positive impacts on a number of existing local shape descriptors.

6-DoF Pose Estimation Performance

A general 6-DoF pose estimation process with local descriptors is achieved by correspondence generation and pose esti-

Table 3: 6-DoF Pose estimation performance on three experimental datasets.

		BR	UWA3M	UWAOR
RANSAC	err_t	0.000	7.929	9.513
	err_r	0.0298	0.696	0.769
LRF-Net	err_t	0.000	6.088	4.392
	err_r	0.0239	0.608	0.405

mation from correspondences with potential outliers [Derpanis, 2010]. RANSAC is arguably the de facto 6-DoF pose estimator in many applications. However, a key limitation of RANSAC is that the computational complexity of RANSAC is $O(n^3)$ and estimating a reasonable pose requires a huge number of iterations. With LRFs, a single correspondence is able to generate a 6-DoF pose, decreasing the computational complexity from $O(n^3)$ to $O(n)$. Therefore, we apply LRF-Net to 6-DoF pose estimation, following a RANSAC-fashion pipeline. The difference is that we sample one correspondence per iteration. Two criteria, i.e., the rotation error err_r between our predicted rotation R and the ground-truth one R_{GT} , and the translation error err_t between the predicted translation vector T and the ground truth one T_{GT} [Mian *et al.*, 2006b], are employed for evaluating the performance of 6-DoF pose estimation.

The initial feature correspondence set is generated by first matching TOLDI (equipped with our LRF-Net) descriptors and keeping 100 correspondences with the highest similarity scores. 100 and 1000 iterations are assigned to our method and RANSAC. The average rotation errors and translation errors of the two estimators on three experimental datasets are shown in Table 3.

Two salient observations can be made from the table. First, both RANSAC and our method manage to achieve accurate pose estimation results on the BR dataset that contains point cloud pairs with large overlapping ratios. However, our method only needs $\frac{1}{10}$ of the iterations required for RANSAC. Second, on more challenging datasets, i.e., UWA3M and UWAOR, our method significantly outperforms RANSAC. This demonstrates that LRF-Net can improve the accuracy and efficiency of RANSAC for 6-DoF pose estimation simultaneously.

3.3 Analysis Experiments

Verifying the Rationality of LRF-Net

To verify the rationality of the main technique components of our LRF-Net, we conduct the following experiments. First, in order to verify the choice of weighted vector-sum operation for x -axis calculation, we test the approach using the vector with the maximum weight as the x -axis (dubbed “Max”). Second, to demonstrate that the axes of LRF is not suitable to be directly regressed, we compare our method with the one regressing x -axis via a network shown in the left of Fig. 8 (dubbed “DR”). The results are shown in the right of Fig. 8.

Clearly, LRF-Net achieves the best performance among tested methods. It verifies that learning weights rather than directly learning axes is more reasonable. In addition, vector-sum is more appropriate for integrating projection vectors with learned weights for LRF-Net.

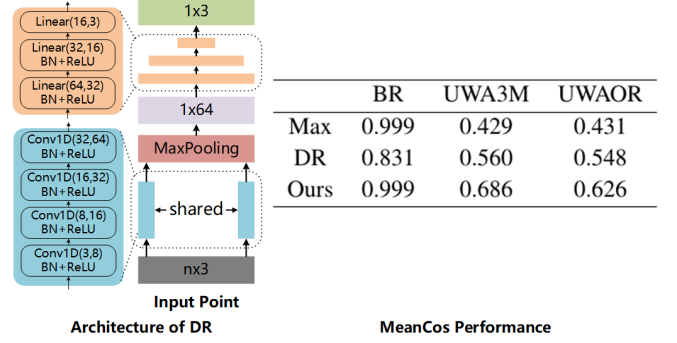


Figure 8: MeanCos performance of LRF-Net and its two variants on three experimental datasets.

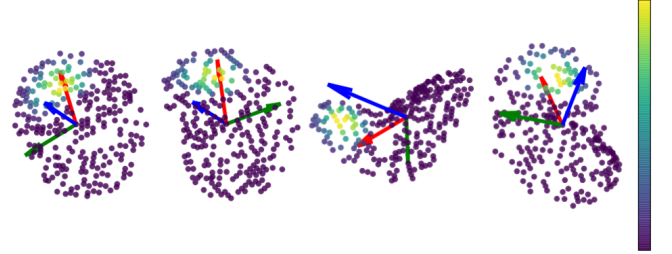


Figure 9: The visualization of the weights for every point in a local surface.

Visualization

Fig. 9 visualizes the learned weights by our LRF-Net for several sample local surfaces, which presents two interesting findings. First, closer points do not seem to have greater contributions. It is a common assumption for many existing CA- and PSD-based LRF methods, including Tombari, Guo, and Yang, that closer points should have greater weights. However, they are inferior to our LRF-Net in terms of repeatability performance. Second, x -axis estimation is generally determined by a particular area, rather than a single salient point as employed by many PSD-based methods, e.g., Petrelli. These visualization results also demonstrate our opinion that each neighboring point in the local surface gives a unique contribution to LRF construction.

4 Conclusion

In this paper, we have proposed LRF-Net, a learned LRF for 3D local surface that is repeatable and robust to a number of nuisances. LRF-Net assumes that each neighboring point in the local surface gives a unique contribution to LRF construction and measure such contributions via learned weights. Experiments showed that our LRF-Net outperforms many state-of-the-art LRF methods on datasets addressing different application scenarios. In addition, LRF-Net can significantly boost the local shape description and 6-DoF pose estimation performance. In the future, we expect further improving the LRF-Net by considering RGB cues and multi-scale geometric information.

References

- [Deng *et al.*, 2018] Haowen Deng, Tolga Birdal, and Slobodan Ilic. Ppf-foldnet: Unsupervised learning of rotation invariant 3d local descriptors. In *Proc. European Conference on Computer Vision*, pages 602–618, 2018.
- [Deng *et al.*, 2019] Haowen Deng, Tolga Birdal, and Slobodan Ilic. 3d local features for direct pairwise registration. *arXiv preprint arXiv:1904.04281*, 2019.
- [Derpanis, 2010] Konstantinos G Derpanis. Overview of the ransac algorithm. *Image Rochester NY*, 4(1):2–3, 2010.
- [Fischler and Bolles, 1981] Martin A Fischler and Robert C Bolles. Random sample consensus: a paradigm for model fitting with applications to image analysis and automated cartography. *Communications of the ACM*, 24(6):381–395, 1981.
- [Gojcic *et al.*, 2019] Zan Gojcic, Caifa Zhou, Jan D Wegner, and Andreas Wieser. The perfect match: 3d point cloud matching with smoothed densities. In *Proc. IEEE International Conference on Computer Vision and Pattern Recognition*, pages 5545–5554, 2019.
- [Guo *et al.*, 2013] Yulan Guo, Ferdous Sohel, Mohammed Bennamoun, Min Lu, and Jianwei Wan. Rotational projection statistics for 3d local surface description and object recognition. *International Journal of Computer Vision*, 105(1):63–86, 2013.
- [Guo *et al.*, 2016] Yulan Guo, Mohammed Bennamoun, Ferdous Sohel, Min Lu, Jianwei Wan, and Ngai Ming Kwok. A comprehensive performance evaluation of 3d local feature descriptors. *International Journal of Computer Vision*, 116(1):66–89, 2016.
- [Malassiotis and Strintzis, 2007] Sotiris Malassiotis and Michael G Strintzis. Snapshots: A novel local surface descriptor and matching algorithm for robust 3d surface alignment. *IEEE Transactions on Pattern Analysis and Machine Intelligence*, 29(7):1285–1290, 2007.
- [Mian *et al.*, 2006a] Ajmal S Mian, Mohammed Bennamoun, and Robyn Owens. Three-dimensional model-based object recognition and segmentation in cluttered scenes. *IEEE Transactions on Pattern Analysis and Machine Intelligence*, 28(10):1584–1601, 2006.
- [Mian *et al.*, 2006b] Ajmal S Mian, Mohammed Bennamoun, and Robyn A Owens. A novel representation and feature matching algorithm for automatic pairwise registration of range images. *International Journal of Computer Vision*, 66(1):19–40, 2006.
- [Mian *et al.*, 2010] Ajmal Mian, Mohammed Bennamoun, and Robyn Owens. On the repeatability and quality of keypoints for local feature-based 3d object retrieval from cluttered scenes. *International Journal of Computer Vision*, 89(2-3):348–361, 2010.
- [Petrelli and Di Stefano, 2011] Alioscia Petrelli and Luigi Di Stefano. On the repeatability of the local reference frame for partial shape matching. In *Proc. IEEE International Conference on Computer Vision*, pages 2244–2251. IEEE, 2011.
- [Petrelli and Di Stefano, 2012] Alioscia Petrelli and Luigi Di Stefano. A repeatable and efficient canonical reference for surface matching. In *Proc. Second International Conference on 3D Imaging, Modeling, Processing, Visualization & Transmission*, pages 403–410. IEEE, 2012.
- [Spezialetti *et al.*, 2019] Riccardo Spezialetti, Samuele Salti, and Luigi Di Stefano. Learning an effective equivariant 3d descriptor without supervision. In *Proc. IEEE International Conference on Computer Vision*, pages 6401–6410, 2019.
- [Tombari *et al.*, 2010] Federico Tombari, Samuele Salti, and Luigi Di Stefano. Unique signatures of histograms for local surface description. In *Proc. European Conference on Computer Vision*, pages 356–369. Springer, 2010.
- [Tombari *et al.*, 2013] Federico Tombari, Samuele Salti, and Luigi Di Stefano. Performance evaluation of 3d key-point detectors. *International Journal of Computer Vision*, 102(1-3):198–220, 2013.
- [Yang *et al.*, 2017] Jiaqi Yang, Qian Zhang, Yang Xiao, and Zhiguo Cao. Toldi: An effective and robust approach for 3d local shape description. *Pattern Recognition*, 65:175–187, 2017.
- [Yang *et al.*, 2018] Jiaqi Yang, Yang Xiao, and Zhiguo Cao. Toward the repeatability and robustness of the local reference frame for 3d shape matching: An evaluation. *IEEE Transactions on Image Processing*, 27(8):3766–3781, 2018.